BIOCHEMISTRY
including biophysical chemistry & molecular biology
Article

Biochemistry **2009,** *48,* 12005–12013 12005
DOI: 10.1021/bi901706w

Reactions of the Flavin Mononucleotide in Complex I: A Combined Mechanism Describes NADH Oxidation Coupled to the Reduction of $APAD^+$, Ferricyanide, or Molecular Oxygen[†]

James A. Birrell, Gregory Yakovlev, and Judy Hirst*

Medical Research Council Mitochondrial Biology Unit, Wellcome Trust/MRC Building, Hills Road, Cambridge CB2 0XY, U.K.

Received October 2, 2009; Revised Manuscript Received November 6, 2009

ABSTRACT: NADH:ubiquinone oxidoreductase (complex I) is a complicated respiratory chain enzyme that conserves the energy from NADH oxidation, coupled to ubiquinone reduction, as a proton motive force across the mitochondrial inner membrane. Alternatively, NADH oxidation, by the flavin mononucleotide in complex I, can be coupled to the reduction of hydrophilic electron acceptors, in non-energy-transducing reactions. The reduction of molecular oxygen and hydrophilic quinones leads to the production of reactive oxygen species, the reduction of nicotinamide nucleotides leads to transhydrogenation, and "artificial" electron acceptors are widely used to study the mechanism of NADH oxidation. Here, we use a combined modeling strategy to accurately describe data from three flavin-linked electron acceptors (molecular oxygen, $APAD^+$, and ferricyanide), in the presence and absence of a competitive inhibitor, ADP-ribose. Our combined ping-pong (or ping-pong-pong) mechanism comprises the Michaelis−Menten equation for the reactions of NADH and $APAD^+$, simple dissociation constants for nonproductive nucleotide−enzyme complexes (defined for specific flavin oxidation states), and second-order rate constants for the reactions of ferricyanide and oxygen. The NADH-dependent parameters are independent of the identity of the electron acceptor. In contrast, a further flavin-linked acceptor, hexaammineruthenium(III), does not obey ping-pong-pong kinetics, and alternative sites for its reaction are discussed. Our analysis provides kinetic and thermodynamic information about the reactions of the flavin active site in complex I that is relevant to understanding the physiologically relevant mechanisms of NADH oxidation and superoxide formation.

NADH:ubiquinone oxidoreductase (complex I) is a complicated, proton-pumping, membrane-bound enzyme, and an entry point for electrons into the respiratory chains of mammalian mitochondria and many other aerobic organisms. The first step in energy transduction by complex I is the oxidation of NADH by a noncovalently bound flavin mononucleotide. Then, the electrons are transferred from the flavin to bound ubiquinone, by a series of iron−sulfur (FeS)[1] clusters, and potential energy from the redox reaction is captured in proton translocation across a membrane. The mechanisms of ubiquinone reduction and proton translocation by complex I remain unknown, but supported by the structure of the hydrophilic domain of complex I from *Thermus thermophilus* (containing the flavin, the NADH binding site, and all of the FeS clusters) (*1*), an understanding of the mechanisms of NADH oxidation and intramolecular electron transfer is emerging. The reactions of the flavin site in complex I, including NADH oxidation and the reduction of molecular oxygen (*2*), a physiologically important side reaction that generates reactive oxygen species and that may lead to cellular oxidative stress (*3*), are the subject of this study.

In complex I, as in many other flavoenzymes, NADH is almost certainly oxidized by a hydride transfer reaction (*4*), preventing formation of the highly unstable $NAD^\bullet$ radical. Recently, structures of the hydrophilic domain of complex I from *T. thermophilus* have been determined with nucleotides bound in the flavin site and reveal the expected juxtaposition of the nicotinamide ring and the flavin isoalloxazine ring system (*5*). During energy transduction, complex I transfers the two electrons from NADH to ubiquinone, but, in vitro, the flavin can be reoxidized by a variety of hydrophilic electron acceptors instead. The hydrophilic electron acceptors do not react at the physiological, hydrophobic, ubiquinone binding site, and their reactions are not energy-transducing (*6*). Here we focus on four such molecules: $APAD^+$ (3-acetylpyridine adenine dinucleotide, an NAD^+ analogue) (*7*, *8*), potassium hexacyanoferrate(III) (ferricyanide or FeCN) (*9*, *10*), hexaammineruthenium(III) chloride (HAR) (*11*), and O_2 (*2*). We consider also the competitive inhibitor ADP-ribose, a truncated form of NADH (or NAD^+) (*12*, *13*). Our aim is to create a unified picture of the reactions catalyzed by the flavin in complex I, by combining data from different reactions in a single analysis (to ensure that every reaction is explained by a universal set of parameters) and by using comprehensive reaction mechanisms (which have not been simplified to linearize data plots in reciprocal analyses). Consequently, we aim to determine (or confirm) the mechanism for each electron acceptor, to improve our understanding of the influence of NADH oxidation on the rate and efficiency of energy transduction by complex I, and to determine kinetic and thermodynamic parameters that can be applied to any reaction at the flavin site.

The transhydrogenation reaction between NADH and $APAD^+$ (and between a range of other nucleotides also) has

[†]This research was supported by The Medical Research Council.

*To whom correspondence should be addressed. Telephone: +44 1223 252810. Fax: +44 1223 252815. E-mail: jh@mrc-mbu.cam.ac.uk.

[1]Abbreviations: FeCN, ferricyanide; FeS, iron−sulfur; HAR, hexaammineruthenium(III); LSQE, least-squares error.

Published on Web 11/09/2009

been described in detail previously (*7*). $APAD^+$ is reduced by hydride transfer from the reduced flavin, in a "ping-pong" reaction that is inhibited by high concentrations of NADH binding to the reduced flavin. FeCN reduction by complex I (and by its flavoprotein subcomplex) is also inhibited by high NADH concentrations (*9*, *10*, *14*), and previous analyses have suggested that FeCN is reduced by the flavin in a "ping-pong-pong" type reaction (*9*). Molecular oxygen reacts with the reduced flavin mononucleotide in complex I in a slow, second-order reaction; the concentration of reduced flavin is set in a pre-equilibrium with NADH and NAD^+ (*2*). However, the kinetics of the reaction have not been studied in detail, and though it is widely assumed that O_2 is reduced only when no nucleotide is bound [consistent with a decrease in the level of O_2 reduction as the NADH concentration is increased (*2*, *15*)], this has yet to be demonstrated explicitly. An alternative is that bound nucleotides modulate O_2 reduction by modulating the flavin's reduction potential, rather than by attenuating the access of O_2 (*13*). In contrast, the NADH−HAR oxidoreduction reaction is not inhibited by NADH, and it has been proposed that HAR oxidizes the reduced flavin while NAD^+ is still bound, by reacting at a different (unknown) site on the enzyme (*11*), or that, for the flavoprotein subcomplex, NADH is oxidized by the protein−HAR complex (*16*). HAR and FeCN probably react differently because of their opposing charges, an idea supported by the differing dependence of their rates on pH (*14*).

EXPERIMENTAL PROCEDURES

Preparation of Complex I from Bovine Heart Mitochondria. Complex I was prepared as described previously (*17*, *18*), concentrated to ~10 mg/mL (determined by the Pierce bicinchoninic acid assay), snap-frozen in liquid nitrogen, and stored at −80 °C.

Kinetic Measurements by UV−Visible Spectroscopy. Assays were conducted at 32 °C in 20 mM Tris-HCl (pH 7.5) in 96-well plates (200 μL) using a Molecular Devices microtiter plate reader. The concentration of complex I was varied to give an appropriate rate for each reaction. NADH, ADP-ribose, $APAD^+$, potassium hexacyanoferrate(III) (ferricyanide, FeCN), and hexaammineruthenium(III) chloride (HAR) were added from concentrated stock solutions in the assay buffer, and all reactions were initiated by the addition of complex I. Initial rates were calculated using linear regression (typically over 15 s), and background rates (in the absence of complex I) were subtracted. NADH:$APAD^+$ transhydrogenation was monitored at 400−450 nm (ε = 3.16 mM^{-1} cm^{-1}) (*7*) and NADH:FeCN and NADH:HAR oxidoreduction at 340−380 nm (ε = 4.81 mM^{-1} cm^{-1}). Superoxide was detected by the reduction of acetylated cytochrome *c* at 550−541 nm (ε = 18.0 mM^{-1} cm^{-1}), and hydrogen peroxide was detected using Amplex Red (Invitrogen) and horseradish peroxidase (Sigma Aldrich) at 557−620 nm (ε = 51.6 mM^{-1} cm^{-1}) (*2*). Each data point is the mean average of at least three independent measurements; standard deviations were calculated for each data point and were always equal to < 10% of the average value.

Data Modeling Procedures. Plots of the initial rate versus substrate concentration were modeled by optimizing the fits between the experimental data and values calculated using steady-state eqs 1−4 (see below). The qualities of the fits calculated using different parameter combinations were assessed both by visual inspection and by calculation of least-squares error (LSQE) values (the sum of the squares of the differences between experimental data points and their equivalent calculated values). We computationally optimized fits by testing a wide range of possible parameter combinations (using programs encoded in C) and choosing the fits with the lowest LSQE values. Combinations of parameter values that gave LSQE values below chosen limits were used to define acceptable parameter ranges.

RESULTS

Complex I Catalyzed Reactions of NADH with $APAD^+$, FeCN, and O_2 Obey Ping-Pong Kinetics. Figure 1 shows data from three reactions catalyzed by complex I: the NADH:$APAD^+$, NADH:FeCN, and NADH:O_2 oxidoreductase reactions (the $APAD^+$, FeCN, and O_2 reactions). It is obvious that all the reactions are inhibited by high concentrations of NADH, and because the $APAD^+$ reaction is known to obey a ping-pong mechanism (in which the two reactants bind at overlapping sites) (*7*), this observation implies that the FeCN and O_2 reactions obey ping-pong-pong mechanisms. NADH and $APAD^+$ react with the flavin mononucleotide in complex I, so the data imply that FeCN and O_2 react with the flavin also, and that NADH binds as an inhibitor when the flavin is reduced and as a substrate when the flavin is oxidized. Conversely, inhibition is not observed at high concentrations of $APAD^+$, FeCN, and O_2, because they are unable to compete effectively with NADH for the oxidized flavin.

The alternating reactions of NADH and $APAD^+$ with the flavin, by hydride transfer mechanisms, have been discussed previously in detail (*7*), so the $APAD^+$ reaction is used here as a basis for describing the FeCN and O_2 data. The stoichiometry of the $APAD^+$ reaction is 1:1, so (in the absence of any participation by the FeS clusters) it involves, alternately, the fully oxidized and fully reduced flavin species. Conversely, FeCN is an obligatory one-electron acceptor, and O_2 is considered here as a one-electron acceptor also, because O_2 reduction by the flavin in *Bos taurus* complex I is known to produce predominantly superoxide (rather than H_2O_2) (*2*). Consequently, the FeCN and O_2 reactions involve the fully oxidized, fully reduced, and semireduced flavin species [in the absence of any participation by the FeS clusters (see below)]. The unified scheme for all three reactions is presented in Scheme 1. Importantly, the three rates of reaction span more than 3 orders of magnitude, the maximum turnover numbers being approximately 200, 2000, and 0.5 NADH s^{-1} for the $APAD^+$, FeCN, and O_2 reactions, respectively (Figure 1). The large range increases the significance of using a common reaction scheme and common sets of parameters to describe all the data sets together.

In Scheme 1, the reactions of NADH and $APAD^+$ are described by the Michaelis−Menten equation, whereas FeCN and O_2 are assumed to undergo simple bimolecular reactions (they do not form specific interactions with the binding site). NADH is a competitive inhibitor because it binds to the reduced flavin (and presumably to the semireduced flavin), as well as to the oxidized flavin. Any inhibition from $APAD^+$, FeCN, or O_2 binding to the oxidized site is extremely weak, and so not included for the sake of simplicity. By using the steady-state approximation for each enzyme intermediate (*19*), eqs 1 and 2 can be derived, to describe the rate of each reaction as a function of its two substrate concentrations.

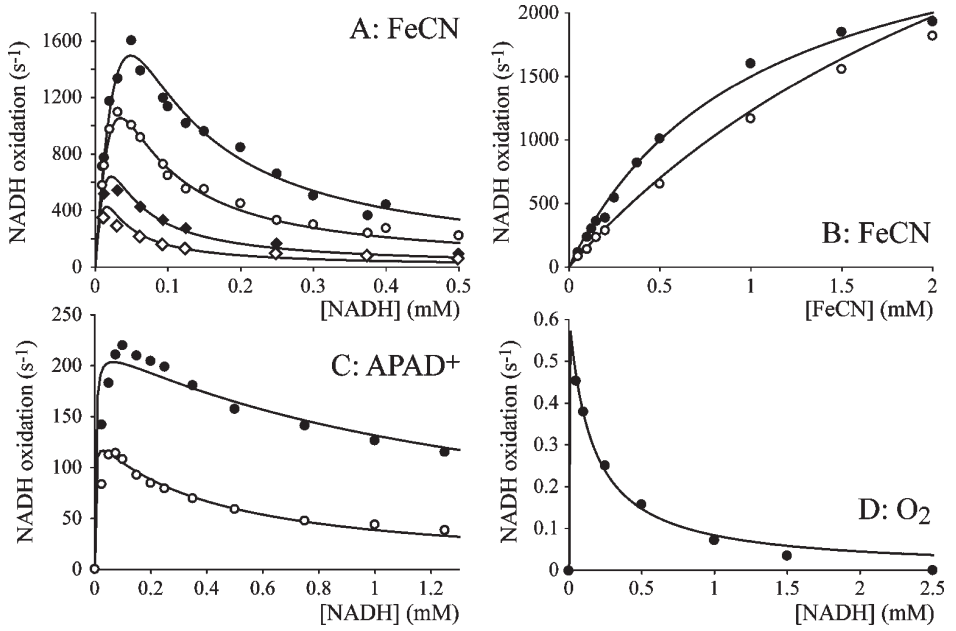

FIGURE 1: Data from the FeCN, $APAD^+$, and O_2 reactions, modeled using Scheme 1 and common values for common parameters. (A) Rate of the FeCN reaction as a function of NADH concentration at four FeCN concentrations: 0.1 (◇), 0.2 (◆), 0.5 (○), and 1 mM (●). (B) Rate of the FeCN reaction as a function of FeCN concentration at two NADH concentrations: 0.05 (●) and 0.1 mM (○). (C) Rate of the $APAD^+$ reaction as a function of NADH concentration at two $APAD^+$ concentrations: 0.25 (○) and 1.5 mM (●) (data presented previously in ref *7*). (D) Rate of the O_2 reaction as a function of NADH concentration in atmospheric O_2. The parameter values used to model the data are from row 1 of Table 1 and were as follows: $K_M^{NADH} = 200\ \mu M$, $k_{cat}^{NADH} = 15000\ s^{-1}$, $(k_{cat}/K_M)^{NADH} = 7.5 \times 10^7\ M^{-1}\ s^{-1}$, $K_{Red}^{NADH} = 200\ \mu M$, $K_{Semi}^{NADH,F} = K_{Semi}^{NADH,O} = 5\ \mu M$, $K_M^{APAD^+} = 240\ \mu M$, $k_{cat}^{APAD^+} = 260\ s^{-1}$, $k_1^{FeCN} = k_2^{FeCN} = 3.7 \times 10^7\ M^{-1}\ s^{-1}$, $k_1^{O_2} = 2.4 \times 10^3\ M^{-1}\ s^{-1}$, and $k_2^{O_2} = 3.7 \times 10^5\ M^{-1}\ s^{-1}$.

$$\text{rate} = ([E]_{TOT} k_{cat}^{NADH}) \Big/ \left[\frac{K_M^{NADH}}{[NADH]} + \frac{k_{cat}^{NADH} K_M^{APAD^+}}{k_{cat}^{APAD^+} [APAD^+]} \left(1 + \frac{[NADH]}{K_{Red}^{NADH}} + \frac{[APAD^+]}{K_M^{APAD^+}} \right) + 1 \right] \quad (1)$$

$$\text{rate} = ([E]_{TOT} k_{cat}^{NADH}) \Big/ \left[\frac{K_M^{NADH}}{[NADH]} + \frac{k_{cat}^{NADH}}{k_1^{FeCN}[FeCN]} \left(1 + \frac{[NADH]}{K_{Red}^{NADH}} \right) + \frac{k_{cat}^{NADH}}{k_2^{FeCN}[FeCN]} \left(1 + \frac{[NADH]}{K_{Semi}^{NADH}} \right) + 1 \right] \quad (2)$$

Equation 1 was used previously to describe the $APAD^+$ reaction (*7*), but a very large number of parameter combinations fit the experimental data successfully, precluding determination of an exact value for any of the parameters. To restrict the number of parameter combinations, the NADH:HAR oxidoreductase reaction was used to estimate K_M^{NADH} and k_{cat}^{NADH}. However, the NADH:HAR oxidoreductase reaction is not inhibited by high concentrations of NADH (see below), so this constraint is not included here. In a similar way, eq 2 (given for FeCN) can be used to model the FeCN and O_2 data sets independently, but a similarly extensive set of parameter combinations applies to these reactions also. Here, we use eqs 1 and 2 to fit the data from all three reactions together, using the same values of K_M^{NADH}, k_{cat}^{NADH}, and K_{Red}^{NADH} in each case. Although individual data fits are optimized slightly less well, the size of the "parameter space" decreases significantly, producing more meaningful estimates of the common parameters. Figure 1 shows one of

Scheme 1: Combination of the Ping-Pong Reaction Mechanisms for the NADH:$APAD^+$, NADH:FeCN, and NADH:O_2 Oxidoreduction Reactions Catalyzed by Complex I[a]

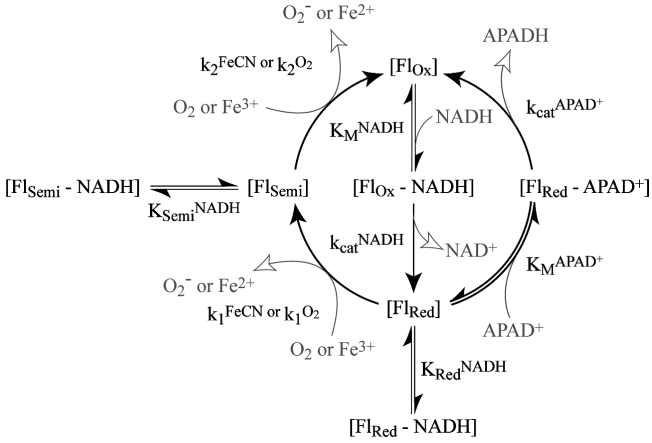

[a]The formation and inhibition of [Fl_{Red}] by NADH (center) are common to all the reactions; the return to [Fl_{Ox}] is dependent on the identity of the electron acceptor.

the "best" fit solutions; a best fit solution is one that displays the minimum combined LSQE value (the sum of the three individual LSQE values, weighted according to the magnitude and number of data points in each of the three data sets).

Because of the large number of best fits that can be produced to explain the data in Figure 1, the "satisfactory" fit approach was taken. Each parameter was screened individually: a value was set for the parameter being screened, and then the combined LSQE value was minimized by allowing all the other parameters to roam freely. If the minimum LSQE value was below the cutoff (1.5 times the best fit value, set chosen by visual inspection of a

Table 1: Allowed Ranges for Each Parameter from Scheme 1, Determined by Combination Modeling of Data from the $APAD^+$, FeCN, and O_2 Reactions[a]

K_M^{NADH} (μM)	k_{cat}^{NADH} (s^{-1})	$(k_{cat}/K_M)^{NADH}$ ($M^{-1}\ s^{-1}$)	K_{Red}^{NADH} (μM)	$K_{Semi}^{NADH,F}$ (μM)	$K_{Semi}^{NADH,O}$ (μM)	$K_M^{APAD^+}$ (μM)	$k_{cat}^{APAD^+}$ (s^{-1})	k_1^{FeCN} ($M^{-1}\ s^{-1}$)	k_2^{FeCN} ($M^{-1}\ s^{-1}$)	$k_1^{O_2}$ ($M^{-1}\ s^{-1}$)	$k_2^{O_2}$ ($M^{-1}\ s^{-1}$)
>47	>5000	5.9×10^7 to 1.2×10^8	100−650	0.20−24	0.20−24	110−570	220−330	$>1.0 \times 10^7$	$>1.0 \times 10^7$	2000−3100	>65000
>47	>5000	5.6×10^7 to 1.2×10^8	78−650	0.20−24	>64	100−580	220−330	$>1.0 \times 10^7$	$>1.0 \times 10^7$	4100−5900	4100−5900
>47	>5000	5.6×10^7 to 1.2×10^8	77−650	0.20−43	$>4.5 \times 10^{-4}$	100−580	220−330	$>6.0 \times 10^6$	$>5.4 \times 10^6$	>2000	>2000

[a] In row 1, $k_1^{FeCN} = k_2^{FeCN}$ and $K_{Semi}^{NADH,F} = K_{Semi}^{NADH,O}$. In row 2, $k_1^{FeCN} = k_2^{FeCN}$ and $k_1^{O_2} = k_2^{O_2}$. In row 3, there are no constraints. Allowed parameter values were those that gave both a combined LSQE value < 1.5 times the minimum value and three individual LSQE values < 2 times their individual minimum values. All values are reported to two significant figures. The maximum values of K_M^{NADH} and $K_{Semi}^{NADH,O}$ (row 3) evaluated were 2000 μM. The maximum value of k_{cat}^{NADH} evaluated was $1 \times 10^5\ s^{-1}$. The second-order rate constants, k_1^{FeCN}, k_2^{FeCN}, $k_1^{O_2}$, and $k_2^{O_2}$, were evaluated up to $1 \times 10^9\ M^{-1}\ s^{-1}$ and not allowed to exceed $1 \times 10^9\ M^{-1}\ s^{-1}$ in evaluation of the other parameters.

range of different fits) and none of the three individual LSQE values were more than twice their individual best fit values, then the value tested was included in the parameter's range. Initially, the constraints $k_1^{FeCN} = k_2^{FeCN}$ and $k_1^{O_2} = k_2^{O_2}$ were applied, to reflect the simple bimolecular nature of the reactions, but no best fit could be obtained by using conserved values for K_M^{NADH}, k_{cat}^{NADH}, K_{Red}^{NADH}, and K_{Semi}^{NADH}. Conversely, excellent fits (see, for example, Figure 1) could be obtained by either allowing the k_1 and k_2 values to vary independently, or by allowing K_{Semi}^{NADH} to adopt different values in the FeCN and O_2 reactions (K_{Semi}^{NADH} is not relevant to the $APAD^+$ reaction). Table 1 presents the ranges for each parameter determined under the three following sets of constraints (note that not every apparent parameter combination from Table 1 will give a satisfactory fit, as relationships between the different parameters exist).

(1) $k_1^{FeCN} = k_2^{FeCN}$, but $k_1^{O_2} \neq k_2^{O_2}$. Allowing both k_1^{FeCN} and k_2^{FeCN}, and $k_1^{O_2}$ and $k_2^{O_2}$, to vary in a manner independent of one another provided excellent fits (see below), but whereas the best fits relied on distinct values for $k_1^{O_2}$ and $k_2^{O_2}$, the values found for k_1^{FeCN} and k_2^{FeCN} were consistently similar. Reintroducing the $k_1^{FeCN} = k_2^{FeCN}$ constraint did not compromise the fits significantly, so it was retained to restrict the number of independent parameters. The most likely explanation stems from the different reduction potentials for Fl_{Ox}/Fl_{Semi} and Fl_{Semi}/Fl_{Red} in complex I: $[Fl_{Semi}]$ is more reducing than $[Fl_{Red}]$ (*20*) so O_2 reacts faster with the semireduced state; O_2 is affected more than FeCN because the reduction potential of O_2 [−0.33 V, to form superoxide, in 1 atm of O_2 (*21*)] is much closer to the flavin's reduction potentials [−0.42 and −0.34 V at pH 7.5 (*20*)] than that of FeCN (0.36 V, measured electrochemically under the experimental conditions used in the assays).

(2) K_{Semi}^{NADH} (FeCN reaction) $\neq K_{Semi}^{NADH}$ (O_2 reaction). In the case of complex I, Scheme 1 is an oversimplification because it does not consider the eight FeS clusters that are able to exchange electrons rapidly with the flavin. The FeS clusters relax the rigid rules by which the three oxidation states of the flavin interconvert in Scheme 1, turning each "flavin oxidation state" into a "set of complex I oxidation states", resulting in a huge increase in the complexity of the underlying scheme. For example, in the presence of NADH only, a typical complex I molecule may be reduced by six electrons: two on the flavin and four on the clusters. Upon reaction with an $APAD^+$ molecule, the four-electron product state probably retains all four electrons on the clusters, conforming to Scheme 1, and alternating between $[Fl_{Red}]$ and $[Fl_{Ox}]$ during the $APAD^+$ reaction. However, when the six-electron state is oxidized by either FeCN or O_2, the resulting five-electron state may contain one electron on the flavin and four on the clusters (as in Scheme 1), or much more likely, the flavin semiquinone may be quenched to give either an oxidized flavin and five electrons on the clusters or a reduced flavin and three electrons on the clusters. NADH may react directly with the oxidized flavin in the former case. Furthermore, the average number of redox electrons in the enzyme is set by the relative rates of oxidation and reduction, so that the molecular identity of the state termed $[Fl_{Semi}]$ in Scheme 1 may differ in steady state during the FeCN and O_2 reactions. The O_2 reaction is slow so $[Fl_{Semi}]$ resembles $[Fl_{Red}]$ more strongly, whereas during the fast FeCN reaction, it resembles $[Fl_{Ox}]$. Although not applied as a constraint in the modeling described here, it is most likely that NADH binds more strongly when the flavin is oxidized than when it is reduced, so that K_{Semi}^{NADH} (FeCN reaction) < K_{Semi}^{NADH} (O_2 reaction).

(3) $k_1^{FeCN} \neq k_2^{FeCN}$, $k_1^{O_2} \neq k_2^{O_2}$, and K_{Semi}^{NADH} (FeCN reaction) $\neq K_{Semi}^{NADH}$ (O_2 reaction). It is possible that both effects described above are operating in complex I, so removing all constraints allows the widest possible satisfactory ranges for each parameter to be explored. The equality between k_1^{FeCN} and k_2^{FeCN} has been removed to acknowledge that, because contributions from the oxidized flavin are nonreactive, the electron delocalization described in the previous paragraph may also affect the reactions of FeCN and O_2. Although not applied as a constraint in the modeling described here, the predominant effect would be to decrease k_2^{FeCN} relative to k_1^{FeCN}.

The Complex I Catalyzed Reaction of NADH with HAR Does Not Obey Ping-Pong Kinetics. HAR is a positively charged, hydrophilic molecule which, like FeCN, accepts electrons rapidly from complex I reduced by NADH. However, as noted previously (*11*), the rate of the NADH:HAR oxidoreductase reaction (the HAR reaction) is not inhibited by high NADH concentrations (see Figure 2A). This observation suggests that the HAR reaction does not follow the ping-pong-pong mechanism of Scheme 1, but because the ping-pong-pong mechanism comprises six independent parameters, it cannot be ruled out by visual inspection alone. Indeed, Scheme 1 and eq 2 can be used to produce an excellent fit to data from the HAR reaction (see Figure 2).

The parameters that provide satisfactory fits to data from the NADH:HAR reaction, according to the ping-pong-pong mechanism in Scheme 1, are summarized in Table 2 (in row 1, $k_1^{HAR} = k_2^{HAR}$; in row 2, $k_1^{HAR} \neq k_2^{HAR}$). The correspondence between the ranges for K_M^{NADH}, k_{cat}^{NADH}, K_{Red}^{NADH}, and K_{Semi}^{NADH} in Tables 1 and 2 is limited. In particular, there is no overlap in the allowed ranges for k_{cat}/K_M^{NADH} (see Figure 2C), suggesting that the two reactions do not share a common mechanism. Consequently, attempts to obtain a satisfactory combined fit to data from the NADH:FeCN and

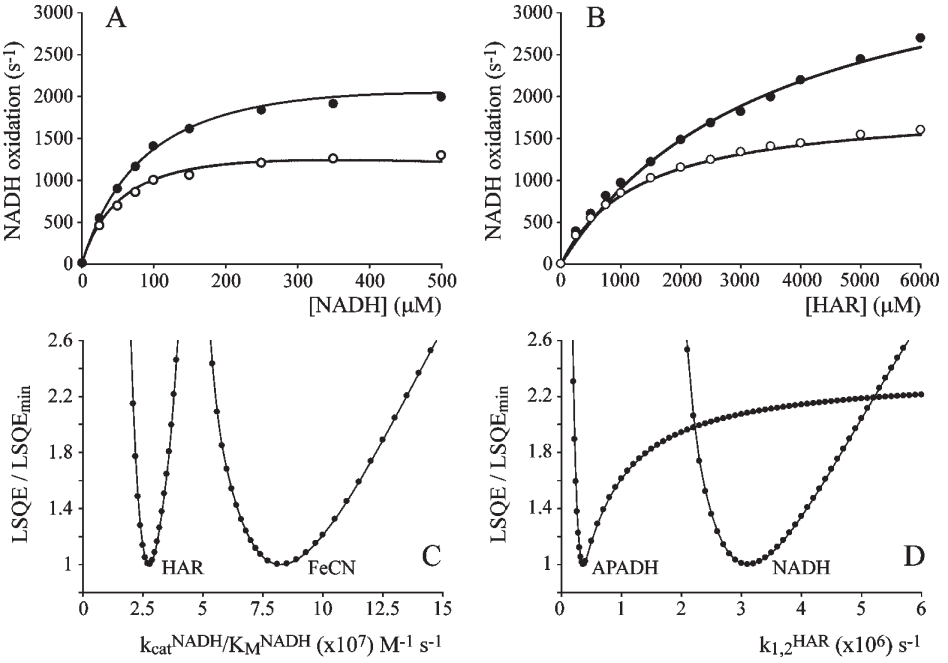

FIGURE 2: Modeling of the NADH:HAR and APADH:HAR oxidoreductase reactions using Scheme 1. (A) Rate of the NADH:HAR reaction as a function of NADH concentration at two HAR concentrations: 1.5 (○) and 3.5 mM (●). (B) Rate of the NADH:HAR reaction as a function of HAR concentration at two NADH concentrations: 100 (○) and 500 μM (●). The parameter values used to model the data in panels A and B are from row 1 of Table 2 and are as follows: $K_M^{NADH} = 210\,\mu M$, $k_{cat}^{NADH} = 5900\,s^{-1}$, $(k_{cat}/K_M)^{NADH} = 2.8 \times 10^7\,M^{-1}\,s^{-1}$, $K_{Red}^{NADH} = 790\,\mu M$, $K_{Semi}^{NADH} = 10$ mM, and $k_1^{HAR} = k_2^{HAR} = 3.1 \times 10^6\,M^{-1}\,s^{-1}$. (C) LSQE values as a function of $(k_{cat}/K_M)^{NADH}$ for the NADH:HAR and NADH:FeCN oxidoreductase reactions. Values for $(k_{cat}/K_M)^{NADH}$ were set, and then the LSQE value was minimized by allowing all other parameters to roam freely. There is no overlap in allowed ranges for the two reactions. No constraints were applied. (D) LSQE values as a function of the $k_1^{HAR} = k_2^{HAR}$ constraint for the NADH:HAR and APADH:HAR oxidoreductase reactions. Values for the $k_1^{HAR} = k_2^{HAR}$ constraint were set, and then the LSQE value was minimized by allowing all other parameters to roam freely. There is no overlap in allowed ranges for the two reactions. No additional constraints were applied.

Table 2: Allowed Ranges for Each Parameter from Scheme 1, Determined by Modeling of Data from the NADH:HAR and APADH:HAR Oxidoreduction Reactions[a]

K_M^{NADH} (μM)	k_{cat}^{NADH} (s^{-1})	$(k_{cat}/K_M)^{NADH}$ ($M^{-1}\,s^{-1}$)	K_{Red}^{NADH} (μM)	K_{Semi}^{NADH} (μM)	k_1^{HAR} ($M^{-1}\,s^{-1}$)	k_2^{HAR} ($M^{-1}\,s^{-1}$)	k_1^{HAR}/k_2^{HAR}
120−420	4300−9600	2.1×10^7 to 3.8×10^7	>210	>210	2.2×10^6 to 5.1×10^6	2.2×10^6 to 5.1×10^6	1
120−420	4300−9600	2.1×10^7 to 3.8×10^7	>0.98	>0.98	$>1.1 \times 10^6$	$>1.1 \times 10^6$	0.0011−890
K_M^{APADH} (μM)	k_{cat}^{APADH} (s^{-1})	$(k_{cat}/K_M)^{APADH}$ ($M^{-1}\,s^{-1}$)	K_{Red}^{APADH} (μM)	K_{Semi}^{APADH} (μM)	k_1^{HAR} ($M^{-1}\,s^{-1}$)	k_2^{HAR} ($M^{-1}\,s^{-1}$)	k_1^{HAR}/k_2^{HAR}
130−500	160−360	6.5×10^5 to 1.3×10^6	>45	>45	2.1×10^5 to 2.4×10^6	2.1×10^5 to 2.4×10^6	1
130−500	160−360	6.5×10^5 to 1.3×10^6	>0.090	>0.090	$>1.0 \times 10^5$	$>1.0 \times 10^5$	5.9×10^{-4} to 9400

[a]In row 1, the NADH:HAR reaction with $k_1^{HAR} = k_2^{HAR}$. In row 2, the NADH:HAR reaction with no constraints. In row 3, the APADH:HAR reaction with $k_1^{HAR} = k_2^{HAR}$. In row 4, the APADH:HAR reaction with no constraints. Allowed parameter values were those that gave an LSQE value < 2 times the minimum value. All values are reported to two significant figures. The maximum values of K_{Red}^{NADH}, K_{Red}^{APADH}, K_{Semi}^{NADH}, and K_{Semi}^{APADH} evaluated were 1 M. The second-order rate constants k_1^{HAR} and k_2^{HAR} (rows 2 and 4) were evaluated up to $1 \times 10^9\,M^{-1}\,s^{-1}$ and not allowed to exceed $1 \times 10^9\,M^{-1}\,s^{-1}$ in evaluation of the other parameters.

NADH:HAR reactions, using common values for K_M^{NADH}, k_{cat}^{NADH}, and K_{Red}^{NADH}, were not successful, even when the chances of obtaining a combined fit were optimized by allowing $k_1^{FeCN} \neq k_2^{FeCN}$, $k_1^{HAR} \neq k_2^{HAR}$, and $K_{Semi}^{NADH,F} \neq K_{Semi}^{NADH,H}$. Furthermore, attempts to obtain good combined fits to data from the NADH:HAR and APADH:HAR reactions using the same values of k_1^{HAR} and k_2^{HAR} [the reaction of HAR with the reduced enzyme should be independent of the identity of the reduced nucleotide (see Scheme 1)] were unsuccessful also, even when the chances of obtaining a combined fit were optimized by allowing $k_1^{HAR} \neq k_2^{HAR}$. Table 2 and Figure 2D show that the overlap between allowed values of $k_{1,2}^{HAR}$ is limited: the best combined fits (based on combining the two individual LSQE values) only just attain satisfactory status, and the favored ranges for the $k_1^{HAR} = k_2^{HAR}$ constraint are clearly different. We conclude that the ping-pong-pong mechanism shown in Scheme 1 is not an appropriate description of the NADH:HAR oxidoreductase reaction mechanism.

Competitive Inhibition at the Flavin Site. ADP-ribose (ADPR) is a known inhibitor of NADH oxidation; it is a truncated form of NADH/NAD^+ that lacks the nicotinamide headgroup (*12*, *13*). Therefore, inhibition of the FeCN, $APAD^+$, and O_2 reactions was used to test the combined ping-pong(-pong) model further, and to determine whether a set of dissociation constants for ADP-ribose and different oxidation states of the flavin could be obtained. Figure 3 presents data from each of the three reactions, inhibited by ADP-ribose and modeled according to Scheme 1 with ADP-ribose binding to each of [Fl_{Ox}], [Fl_{Semi}], and [Fl_{Red}] (K_{Ox}^{ADPR}, K_{Semi}^{ADPR}, and K_{Red}^{ADPR}).

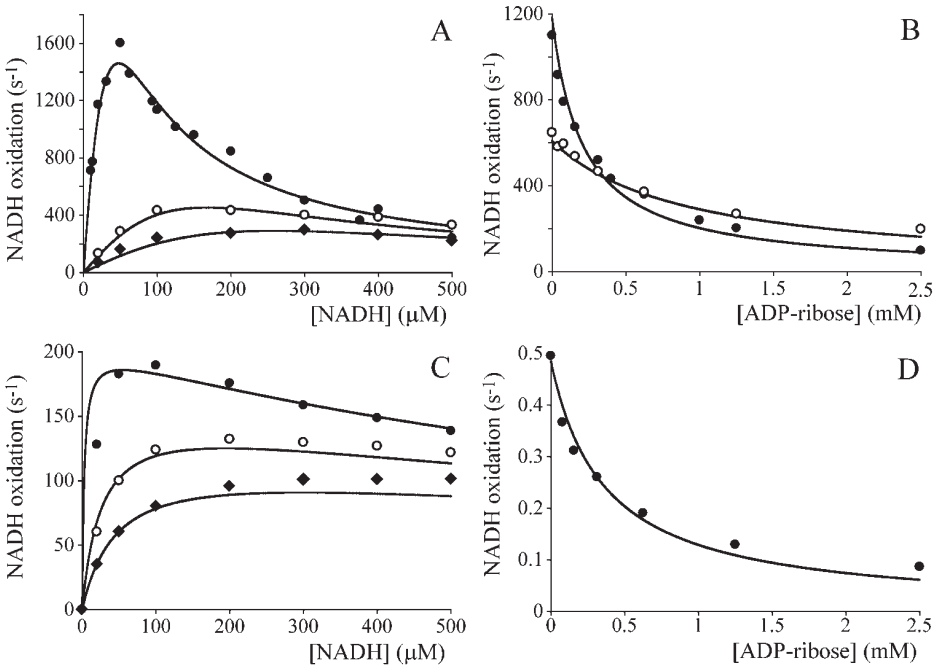

FIGURE 3: Data from the FeCN, $APAD^+$, and O_2 reactions inhibited with ADP-ribose, modeled using Scheme 1 and common values for common parameters. (A) Rate of the FeCN reaction as a function of NADH concentration at three ADP-ribose concentrations: 1 (◆), 0.4 (○), and 0 mM (●) ([FeCN] = 1 mM). (B) Rate of the FeCN reaction as a function of ADP-ribose concentration at two NADH concentrations: 0.1 (●) and 0.25 mM (○) ([FeCN] = 1 mM). (C) Rate of the $APAD^+$ reaction as a function of NADH concentration at three ADP-ribose concentrations: 1 (◆), 0.4 (○), and 0 mM (●) ([$APAD^+$] = 1 mM). (D) Rate of the O_2 reaction as a function of ADP-ribose concentration in 30 μM NADH and atmospheric O_2. The parameter values used to model the data are from row 3 of Table 3 and provided excellent fits to all data recorded in the absence of ADP-ribose also: ${K_M}^{NADH} = 340\ \mu M$, $({k_{cat}}/{K_M})^{NADH} = 7.5 \times 10^7\ M^{-1}\ s^{-1}$, ${K_{Red}}^{NADH} = 250\ \mu M$, ${K_{Semi}}^{NADH,F} = 8\ \mu M$, ${K_{Semi}}^{NADH,O} = 140\ \mu M$, ${K_M}^{APAD^+} = 290\ \mu M$, ${k_{cat}}^{APAD^+} = 270\ s^{-1}$, ${k_1}^{FeCN} = 2.5 \times 10^7\ M^{-1}\ s^{-1}$, ${k_2}^{FeCN} = 2.2 \times 10^7\ M^{-1}\ s^{-1}$, ${k_1}^{O_2} = 4.5 \times 10^3\ M^{-1}\ s^{-1}$, ${k_2}^{O_2} = 4.5 \times 10^5\ M^{-1}\ s^{-1}$, ${K_{Red}}^{ADPR} = 310\ \mu M$, ${K_{Semi}}^{ADPR,F} = {K_{Semi}}^{ADPR,O} = 310\ \mu M$, and ${K_{Ox}}^{ADPR} = 35\ \mu M$.

Equations 3 and 4 refer to the ping-pong ($APAD^+$) and ping-pong-pong (FeCN and O_2) reactions, respectively.

$$\text{rate} = ([E]_{TOT}{k_{cat}}^{NADH}) \Big/ \left[\frac{{K_M}^{NADH}}{[NADH]}\left(1+\frac{[ADPR]}{{K_{Ox}}^{ADPR}}\right) + \frac{{k_{cat}}^{NADH}{K_M}^{APAD^+}}{{k_{cat}}^{APAD^+}[APAD^+]}\left(1+\frac{[NADH]}{{K_{Red}}^{NADH}}+\frac{[APAD^+]}{{K_M}^{APAD^+}} + \frac{[ADPR]}{{K_{Red}}^{ADPR}}\right)+1\right] \quad (3)$$

$$\text{rate} = ([E]_{TOT}{k_{cat}}^{NADH}) \Big/ \left[\frac{{K_M}^{NADH}}{[NADH]}\left(1+\frac{[ADPR]}{{K_{Ox}}^{ADPR}}\right) + \frac{{k_{cat}}^{NADH}}{{k_1}^{FeCN}[FeCN]}\left(1+\frac{[NADH]}{{K_{Red}}^{NADH}}+\frac{[ADPR]}{{K_{Red}}^{ADPR}}\right) + \frac{{k_{cat}}^{NADH}}{{k_2}^{FeCN}[FeCN]}\left(1+\frac{[NADH]}{{K_{Semi}}^{NADH}}+\frac{[ADPR]}{{K_{Semi}}^{ADPR}}\right)+1\right] \quad (4)$$

The number of independently variable parameters in eqs 3 and 4 has increased by three, from 11 in eqs 1 and 2, already a significant number. First, in rows 1 and 2 of Table 1, constraints were applied to decrease the number of parameters (to nine in each case) and analogous constraints are applied in rows 1 and 2 of Table 3, also. In row 1, ${k_1}^{FeCN} = {k_2}^{FeCN}$, ${K_{Semi}}^{NADH,F} = {K_{Semi}}^{NADH,O}$, and ${K_{Semi}}^{ADPR,F} = {K_{Semi}}^{ADPR,O}$, and in row 2, ${k_1}^{FeCN} = {k_2}^{FeCN}$ and ${k_1}^{O_2} = {k_2}^{O_2}$. None of these constraints were applied to row 3. Second, in all three rows of Table 1, $({k_{cat}}/{K_M})^{NADH}$ gave a minimum error value at $7.5 \times 10^7\ M^{-1}\ s^{-1}$, and both K_M and k_{cat} exhibited "threshold values", below which the LSQE value increases sharply and above which it is independent of the value tested. Therefore, $({k_{cat}}/{K_M})^{NADH}$ was constrained to $7.5 \times 10^7\ M^{-1}\ s^{-1}$ for Table 3. Although the reaction of $APAD^+$ cannot be described by a second-order rate constant, a relationship between ${K_M}^{APAD^+}$ and ${k_{cat}}^{APAD^+}$ was observed in all three rows of Table 1 also (${k_{cat}}^{APAD^+} = {K_M}^{APAD^+} \times 174000 + 220$), and it was used to further reduce the number of independent parameters in eqs 3 and 4. Third, allowing ${K_{Semi}}^{ADPR}$ (or ${K_{Semi}}^{ADPR,F}$ and ${K_{Semi}}^{ADPR,O}$) to vary independently allowed them to adopt unreasonably high values (≤1 M) that were out of the range of ${K^{ADPR}}_{Ox}$ and ${K^{ADPR}}_{Red}$. Therefore, in all three rows of Table 3, they were confined to lie between (or to equal) ${K_{Ox}}^{ADPR}$ and ${K_{Red}}^{ADPR}$. Table 3 reports the satisfactory ranges for the NADH- and ADP-ribose-dependent parameters, determined by using eqs 3 and 4 to model the entire data set (all three reactions, inhibited and noninhibited), under the constraints described. As described above, a fit was deemed satisfactory if the minimum combined LSQE value was less than 1.5 times the best fit value, and if none of the individual LSQE values were more than 2 times their individual best fit values. It is important to note that, with six independent error values, different methods of weighting the contributions to a combined error value may produce variations in the limits of the parameter ranges reported, and that the ranges for the NADH-dependent parameters are narrowed from those reported in Table 1, as the ADP-ribose data impose additional constraints.

DISCUSSION

Mechanisms of the FeCN, $APAD^+$, O_2, and HAR Reactions. The successful combined analysis of data from the

Table 3: Allowed Ranges for the NADH and ADP-ribose Parameters from Scheme 1 in the Presence of an Inhibitor, Determined by Combination Modeling of Data from the $APAD^+$, FeCN, and O_2 Reactions[a]

K_M^{NADH} (μM)	$K_{Semi}^{NADH,F}$ (μM)	$K_{Semi}^{NADH,O}$ (μM)	K_{Red}^{NADH} (μM)	K_{Ox}^{ADPR} (μM)	$K_{Semi}^{ADPR,F}$ (μM)	$K_{Semi}^{ADPR,O}$ (μM)	K_{Red}^{ADPR} (μM)
> 190	0.20−15	0.20−15	120−520	28−56	72−480	72−480	230−530
> 210	0.20−15	> 77	85−520	28−56	40−920	150−480	230−1000
> 210	0.20−29	$> 5.5 \times 10^{-4}$	85−520	28−56	40−920	28−480	230−1000

[a] In row 1, $k_1^{FeCN} = k_2^{FeCN}$, $K_{Semi}^{NADH,F} = K_{Semi}^{NADH,O}$, and $K_{Semi}^{ADPR,F} = K_{Semi}^{ADPR,O}$. In row 2, $k_1^{FeCN} = k_2^{FeCN}$ and $k_1^{O_2} = k_2^{O_2}$. In row 3, no constraints. In all cases, $k_{cat}^{NADH}/K_M^{NADH} = 7.5 \times 10^7\ M^{-1}\ s^{-1}$ and $k_{cat}^{APAD^+} = 174000 K_M^{APAD^+} + 220$. Allowed parameter values were those that gave both a combined LSQE value of < 1.5 times the minimum value, and six individual LSQE values < 2 times their individual minimum values. All values are reported to two significant figures. The maximum values of K_M^{NADH} and $K_{Semi}^{NADH,O}$ (row 2) evaluated were 2000 μM. The second-order rate constants, k_1^{FeCN}, k_2^{FeCN}, $k_1^{O_2}$, and $k_2^{O_2}$, were evaluated up to $1 \times 10^9\ M^{-1}\ s^{-1}$ and not allowed to exceed $1 \times 10^9\ M^{-1}\ s^{-1}$ in the evaluation of the other parameters.

FeCN, $APAD^+$, and O_2 reactions, despite their very different rates, strongly supports Scheme 1 as an appropriate description of their mechanisms. Scheme 1 shows that the $APAD^+$ reaction occurs by a ping-pong mechanism, in which NADH competitively inhibits the reduction of $APAD^+$, and that the FeCN and O_2 reactions occur by ping-pong-pong mechanisms, in which NADH inhibits the reduction of both FeCN and O_2. Thus, our conclusions are in agreement with previous work on $APAD^+$ (*7*) and FeCN (*9*). It is most likely that NADH inhibits the reduction of $APAD^+$, FeCN, and O_2 simply by blocking their interaction with the reduced enzyme, suggesting strongly that $APAD^+$, FeCN, and O_2 are all reduced directly by the flavin, but only when no nucleotide is bound. In contrast, although kinetic data from the HAR reaction can be modeled accurately using the ping-pong-pong mechanism of Scheme 1, it is not possible to combine analysis of the HAR reaction with analysis of the three established ping-pong(-pong) reactions. It is this mismatch, and the mismatched parameter ranges from the NADH:HAR and APADH:HAR reactions, that excludes the ping-pong-pong mechanism for the HAR reaction. Previous kinetic analyses suggested that the HAR reaction is "ordered" (*11*), but the molecular mechanism behind the ordering remains unclear. The distinction among HAR, FeCN, and O_2 probably arises from their different charges; HAR is positively charged, FeCN negatively charged, and O_2 neutral. A set of hydrophilic quinones have recently been shown to react by a ping-pong or ping-pong-pong mechanism, and they are also uncharged (*22*). The hydrophilic quinones are excluded from the combined analysis because it is not known whether they are reduced by one or two electrons and because their effective concentrations in solution are difficult to define, due to the formation of micelles.

The pseudo-first-order rate constant for HAR reduction by complex I is $> 6 \times 10^3\ s^{-1}$ [$1 \times 10^6\ M^{-1}\ s^{-1}$ (Table 2, row 2) × 0.006 M (the highest HAR concentration studied)]. To achieve this rate, the Ru^{3+} ion must approach to within 15.6 Å of its reductant [using Dutton's equation (*23*) with $\Delta G = -\lambda$, zero distance defined at ionic contact]. By using a 3.6 Å diameter probe to represent the HAR molecule, the surface of the seven core subunits in the nucleotide-bound *T. thermophilus* structure [PDB entry 3IAM (*5*)] was scanned using the program Surface from the CCP4 suite (*24*−*26*), and the closest approaches of the Ru^{3+} to each cluster were calculated. For seven clusters, the Ru^{3+} can approach to within 15.6 Å (all except the second cluster in TYKY), and for two clusters (the histidine-ligated cluster in the 75 kDa subunit and the adjacent cluster in TYKY), it can approach to within 10 Å. Although the seven hydrophilic core subunits are closely related in *T. thermophilus* and *B. taurus*, *B. taurus* complex I also contains a number of additional subunits: our structural analysis is limited, but it establishes the possibility that HAR accepts electrons from one of the clusters. HAR reacts with the flavoprotein subcomplex of complex I (*16*); therefore, it may accept electrons from the [2Fe-2S] cluster in the 24 kDa subunit or the [4Fe-4S] cluster in the 51 kDa subunit, and it probably binds at a negatively charged site (*14*). However, HAR cannot approach to within 15.6 Å of any cluster if it binds in the negatively charged groove adjacent to the large domain of the 75 kDa subunit in *T. thermophilus* (*27*).

Evaluation of the Methodology for the Determination of Kinetic and Thermodynamic Parameters. The steady-state modeling approach described here allows any kinetic mechanism to be applied in interpreting experimental data; the choice is not restricted to only mechanisms that can be linearized in reciprocal data plots (to determine parameters from points of intersection and straight-line gradients). Therefore, all the important kinetic determinants may be considered (although an overly complex mechanism inevitably leads to individual parameters being less well-defined). Here, it is important to define the oxidation state of the flavin at each point in the reaction, so that nucleotide dissociation constants can be defined separately for each state. Overlooking this requirement in the past has led to proposals for more than one nucleotide binding site in complex I (*8*), but it is now clear that a single nucleotide binding site is sufficient to explain all extant data (see also ref *13*). Mechanisms that are too simple may also complicate interpretation of parameters such as K_M or k_{cat}. The maximum rates of reaction described here vary over 4 orders of magnitude, and the apparent K_M^{NADH} values vary from < 0.1 μM for O_2 (*2*) to ~10 μM or more for FeCN and $APAD^+$, but the same underlying K_M^{NADH} and k_{cat}^{NADH} values are identified in the combined analysis, which makes K_M^{NADH} and k_{cat}^{NADH} independent of the electron acceptor and which precludes incompatible values being produced in separate analyses. Finally, our modeling approach recognizes the fact that the data cannot necessarily distinguish a specific value for every parameter and, instead, allows a set of satisfactory ranges to be determined, to describe the possible values for each parameter that are consistent with the data set.

Interpretation of Kinetic and Thermodynamic Parameters and Comparison with Reported Values. K_M^{NADH} and k_{cat}^{NADH} are defined explicitly in Scheme 1, to be independent of the reactions of $APAD^+$, FeCN, and O_2, and our data modeling suggests that $K_M^{NADH} > 50\ \mu M$ and $k_{cat}^{NADH} > 5000\ s^{-1}$ (Table 1). Inclusion of the ADP-ribose data raises their lower limits further, to $K_M^{NADH} > 200\ \mu M$ and $k_{cat}^{NADH} > 15000\ s^{-1}$ (Table 3). In either case, the data are consistent with a $k_{cat}^{NADH}/K_M^{NADH}$ value of $\sim 7.5 \times 10^7\ M^{-1}\ s^{-1}$, a value that approaches the lower limit expected of a diffusion-controlled enzyme-catalyzed reaction (*28*); NADH binding to produce the Michaelis complex is unlikely to limit the rate of turnover.

To interpret the values of K_M^{NADH} and k_{cat}^{NADH} further, it is necessary to resolve them into their constituents; indeed, even NADH binding to the oxidized flavin is unlikely to be defined by a single transition state (*29*). Importantly, k_{cat}^{NADH} includes both reversible hydride transfer and NAD^+ dissociation (rendered irreversible by the absence of NAD^+ in the bulk solution), so the first-order rate constants for "forward" hydride transfer and dissociation of NAD^+ from the reduced flavin must both be greater than 15000 s^{-1}. The much studied hydride transfer catalyzed by dihydrofolate reductase is governed by enzyme dynamics and occurs at ~950 s^{-1} (*30*), but much faster hydride transfer reactions have also been reported [for example, ~2 × 10^4 s^{-1} in proton translocating transhydrogenase (*31*) and ~2 × 10^6 s^{-1} in protochlorophyllide oxidoreductase (*32*)]. Therefore, it is not possible to identify a single rate-limiting step in NADH oxidation by complex I at present. There have been few previous estimations of the rates of the reactions that comprise NADH oxidation by complex I. Recently, freeze-quench EPR was used to show that NADH reacts with complex I from *Escherichia coli* within ~90 μs (~8000 s^{-1}) and that a second reaction occurs after ~1 ms (~700 s^{-1}) (*33*); the first reaction is probably limited by either NADH binding or hydride transfer and the second by dissociation of NAD^+ from the oxidized flavin. The results suggest that turnover may be limited by NAD^+ dissociation, but the values are difficult to compare directly because the FeCN reaction is slower in *E. coli* complex I than in *B. taurus* complex I.

The dissociation constants for nucleotides from the flavin in complex I remain poorly defined. In principle, K_M^{NADH} contains information about K_{Ox}^{NADH}, because $K_M \geq K_D$, but $K_M^{NADH} >$ 200 μM so K_{Ox}^{NADH} can take any value. The idea that NADH binds "tightly" to complex I when the flavin is oxidized has arisen from inappropriate consideration of apparent K_M values from multistep reactions (for example, refs *27* and *34*) and may or may not be correct. By considering a more complex reaction scheme for NADH oxidation, Vinogradov has estimated that $K_{Ox}^{NADH} \leq$ 100 μM, but this estimation is still based on varying "k_{cat}" by varying the concentration of the electron acceptor (*35*). There is better agreement on K_{Red}^{NADH}, which has been estimated to be 20 μM (*13*), 20 or 50 μM (*35*), 50 μM (*9*), 160−260 μM (*7*), or 80 μM (*34*). To the best of our knowledge, there are no reported values for K_{Semi}^{NADH}, but as discussed above, K_{Semi}^{NADH} is convoluted and the molecular identity of the semireduced state is poorly defined (similar comments apply to K_{Semi}^{ADPR}). There is good agreement, however, for the dissociation constants of ADP-ribose. The previously reported values [K_{Ox}^{ADPR} = 25−30 μM, and K_{Red}^{ADPR} = 400−500 μM (*12*, *13*, *35*)] are well within the ranges defined here. Interestingly, ADP-ribose binds more strongly when the flavin is oxidized, suggesting that the negative charge of the reduced flavin decreases its affinity by electrostatic interactions with the phosphates. If the same effect contributes to the determination of the dissociation constants of NADH and NAD^+, then K_{Ox}^{NADH} would be estimated to be between 2 and 50 μM, and from the generally accepted estimate for $K_{Ox}^{NAD^+}$ of ~1 mM (*35*), $K_{Red}^{NAD^+}$ would be estimated to be ~10 mM. Mutation of the conserved glutamate in the flavin site in *E. coli* complex I has supported the idea that a local negative charge decreases nucleotide binding affinities (*36*), but charge is clearly not the whole story, because the positively charged nicotinamide ring of NAD^+ actually serves to decrease its affinity ($K_{Ox}^{NAD^+}$ of ~1 mM compared to K_{Ox}^{ADPR} of 25−30 μM).

Implications for Complex I in the Mitochondrion. The direct participation of the reduced flavin in the reduction of O_2 by complex I has been demonstrated thermodynamically [in the absence of any other electron acceptor, the rate is defined by the NADH/NAD^+ ratio and hence by the fraction of the flavin that is in the fully reduced state (*2*)]; similar dependencies of O_2 reduction on NADH/NAD^+ ratio have been reported for complex I in the mitochondrion (*37*, *38*). However, there is little direct information about how O_2 reduction is affected by the flavin site occupancy, and hence by the NADH and NAD^+ concentrations. Although the recently determined nucleotide-bound structure of the hydrophilic domain of complex I from *T. thermophilus* suggests that the access of O_2 to the reduced flavin is blocked by bound nucleotides, there is no clear correlation between the flavin accessibility and the rate of O_2 reduction in a range of flavoenzymes (*39*). Here, we demonstrate explicitly that nucleotide binding decreases the rate of O_2 reduction by the reduced flavin in complex I, and our data are fully consistent with bound nucleotide preventing O_2 access. An alternative possibility, that bound nucleotides modulate the rate of O_2 reduction via the flavin's reduction potential (*13*), can now be excluded: the extent of inhibition by ADP-ribose cannot be explained by the ~30 mV potential shift that results from a 10-fold higher affinity for the oxidized flavin (relative to the reduced flavin), and our ability to explain data from the $APAD^+$ and FeCN reactions alongside the O_2 reaction ($APAD^+$ must be blocked by nucleotide binding, and these two reactions do not depend so explicitly on the NADH/NAD^+ ratio) confirms that this explanation is not predominant. In any case, our observations further confirm the direct participation of the reduced flavin in the O_2 reduction reaction. Finally, high concentrations of both NADH and NAD^+ are present in the mitochondrial matrix. The total concentration is approximately 3 mM; ~300 μM is present as NADH under typical conditions, but binding to other proteins also affects the concentrations of the free nucleotides (*40*−*43*). Figure 1 shows that 300 μM NADH exerts a significant inhibitory effect on O_2 reduction, so the effects of nucleotide binding must be included in comparisons of superoxide production by isolated complex I and complex I in the mitochondrion. Furthermore, predicted rates of O_2 reduction by the flavin in complex I under "physiological conditions" (the NAD^+ pool is 90% oxidized, the NADH concentration is 300 μM, and the O_2 concentration is low) are essentially negligible: physiologically, ROS production by the flavin site in complex I can be significant only when the NAD^+ potential drops.

Clearly, NADH oxidation by the flavin is crucial for energy transduction by complex I because it delivers the electrons for ubiquinone reduction, but how relevant is a structural, thermodynamic, and kinetic understanding of the mechanism of the flavin-catalyzed reaction to understanding the complete mechanism of energy transduction? First, NADH oxidation is much faster than quinone reduction, so that NADH oxidation does not limit catalysis. Second, energy transduction by complex I is reversible (the conversion of ΔE into Δp is efficient), so the potential energy from NADH oxidation must be conserved; different states of the flavin site (oxidized or reduced, occupied or unoccupied) possess different levels of potential energy, so "control" over which states are visited may be important in energy conservation. Finally, the two "half-reactions" of NADH oxidation and ubiquinone reduction must be tightly coupled, and thus, it may not be possible to dissect the energy transduction mechanism cleanly into sections: information about the rate-limiting steps and reaction intermediates of the NADH oxidation

reaction is a crucial part of building an understanding of the complete mechanism of energy transduction by complex I.

REFERENCES

1. Sazanov, L. A., and Hinchliffe, P. (2006) Structure of the hydrophilic domain of respiratory complex I from *Thermus thermophilus*. *Science 311*, 1430–1436.
2. Kussmaul, L., and Hirst, J. (2006) The mechanism of superoxide production by NADH:ubiquinone oxidoreductase (complex I) from bovine heart mitochondria. *Proc. Natl. Acad. Sci. U.S.A. 103*, 7607–7612.
3. Murphy, M. P. (2009) How mitochondria produce reactive oxygen species. *Biochem. J. 417*, 1–13.
4. Fraaije, M. W., and Mattevi, A. (2000) Flavoenzymes: Diverse catalysts with recurrent features. *Trends Biochem. Sci. 25*, 126–132.
5. Berrisford, J. M., and Sazanov, L. A. (2009) Structural basis for the mechanism of respiratory complex I. *J. Biol. Chem. 284*, 29773–29783.
6. Vinogradov, A. D. (1998) Catalytic properties of the mitochondrial NADH-ubiquinone oxidoreductase (complex I) and the pseudo-reversible active/inactive enzyme transition. *Biochim. Biophys. Acta 1364*, 169–185.
7. Yakovlev, G., and Hirst, J. (2007) Transhydrogenation reactions catalyzed by mitochondrial NADH-ubiquinone oxidoreductase (complex I). *Biochemistry 46*, 14250–14258.
8. Zakharova, N. V., Zharova, T. V., and Vinogradov, A. D. (1999) Kinetics of transhydrogenase reaction catalyzed by the mitochondrial NADH-ubiquinone oxidoreductase (complex I) imply more than one catalytic nucleotide-binding sites. *FEBS Lett. 444*, 211–216.
9. Dooijewaard, G., and Slater, E. C. (1976) Steady-state kinetics of high molecular weight (type I) NADH dehydrogenase. *Biochim. Biophys. Acta 440*, 1–15.
10. Minakami, S., Ringler, R. L., and Singer, T. P. (1962) Studies on the respiratory chain-linked dihydrodiphosphopyridine nucleotide dehydrogenase. *J. Biol. Chem. 237*, 569–576.
11. Sled, V. D., and Vinogradov, A. D. (1993) Kinetics of the mitochondrial NADH-ubiquinone oxidoreductase interaction with hexaammineruthenium III. *Biochim. Biophys. Acta 1141*, 262–268.
12. Zharova, T. V., and Vinogradov, A. D. (1997) A competitive inhibition of the mitochondrial NADH-ubiquinone oxidoreductase (complex I) by ADP-ribose. *Biochim. Biophys. Acta 1320*, 256–264.
13. Grivennikova, V. G., Kotlyar, A. B., Karliner, J. S., Cecchini, G., and Vinogradov, A. D. (2007) Redox-dependent change of nucleotide affinity to the active site of the mammalian complex I. *Biochemistry 46*, 10971–10978.
14. Zickermann, V., Kurki, S., Kervinen, M., Hassinen, I., and Finel, M. (2000) The NADH oxidation domain of complex I: Do bacterial and mitochondrial enzymes catalyze ferricyanide reduction similarly? *Biochim. Biophys. Acta 1459*, 61–68.
15. Vinogradov, A. D., and Grivennikova, V. G. (2005) Generation of superoxide radical by the NADH:ubiquinone oxidoreductase of heart mitochondria. *Biochemistry* (*Moscow, Russ. Fed.*) *70*, 120–127.
16. Gavrikova, E. V., Grivennikova, V. G., Sled, V. D., Ohnishi, T., and Vinogradov, A. D. (1995) Kinetics of the mitochondrial three-subunit NADH-dehydrogenase interaction with hexaammineruthenium III. *Biochim. Biophys. Acta 1230*, 23–30.
17. Sharpley, M. S., Shannon, R. J., Draghi, F., and Hirst, J. (2006) Interactions between phospholipids and NADH:ubiquinone oxidoreductase (complex I) from bovine mitochondria. *Biochemistry 45*, 241–248.
18. Sherwood, S., and Hirst, J. (2006) Investigation of the mechanism of proton translocation by NADH:ubiquinone oxidoreductase (complex I) from bovine heart mitochondria: Does the enzyme operate by a Q-cycle mechanism? *Biochem. J. 400*, 541–550.
19. Briggs, G. E., and Haldane, J. B. S. (1925) A note on the kinetics of enzyme action. *Biochem. J. 19*, 338–339.
20. Sled, V. D., Rudnitzky, N. I., Hatefi, Y., and Ohnishi, T. (1994) Thermodynamic analysis of flavin in mitochondrial NADH:ubiquinone oxidoreductase (complex I). *Biochemistry 33*, 10069–10075.
21. Wood, P. M. (1988) The potential diagram for oxygen at pH 7. *Biochem. J. 253*, 287–289.
22. King, M. S., Sharpley, M. S., and Hirst, J. (2009) Reduction of hydrophilic ubiquinones by the flavin in mitochondrial NADH: ubiquinone oxidoreductase (complex I) and production of reactive oxygen species. *Biochemistry 48*, 2053–2062.
23. Page, C. C., Moser, C. C., Chen, X., and Dutton, P. L. (1999) Natural engineering principles of electron tunnelling in biological oxidation-reduction. *Nature 402*, 47–52.
24. Collaborative Computational Project, Number 4 (1994) The CCP4 suite: Programs for protein crystallography. *Acta Crystallogr. D50*, 760–763.
25. Lee, B., and Richards, F. M. (1971) The interpretation of protein structures: Estimation of static accessibility. *J. Mol. Biol. 55*, 379–400.
26. Chothia, C. (1975) Structural invariants in protein folding. *Nature 254*, 304–308.
27. Sazanov, L. A. (2007) Respiratory complex I: Mechanistic and structural insights provided by the crystal structure of the hydrophilic domain. *Biochemistry 46*, 2275–2288.
28. Stroppolo, M. E., Falconi, M., Caccuri, A. M., and Desideri, A. (2001) Superefficient enzymes. *Cell. Mol. Life Sci. 58*, 1451–1460.
29. Deng, H., Zhadin, N., and Callender, R. (2001) Dynamics of protein ligand binding on multiple time scales: NADH binding to lactate dehydrogenase. *Biochemistry 40*, 3767–3773.
30. Benkovic, S. J., and Hammes-Schiffer, S. (2003) A perspective on enzyme catalysis. *Science 301*, 1196–1202.
31. Pinheiro, T. J. T., Venning, J. D., and Jackson, J. B. (2001) Fast hydride transfer in proton-translocating transhydrogenase revealed in a rapid mixing continuous flow device. *J. Biol. Chem. 276*, 44757–44761.
32. Heyes, D. J., Sakuma, M., de Visser, S. P., and Scrutton, N. S. (2009) Nuclear quantum tunneling in the light-activated enzyme protochlorophyllide oxidoreductase. *J. Biol. Chem. 284*, 3762–3767.
33. Verkhovskaya, M. L., Belevich, G., Euro, L., Wikström, M., and Verkhovsky, M. I. (2008) Real-time electron transfer in respiratory complex I. *Proc. Natl. Acad. Sci. U.S.A. 105*, 3763–3767.
34. Avraam, R., and Kotlyar, A. B. (1991) Kinetics of NADH oxidation and NAD^+ reduction by mitochondrial complex I. *Biochemistry* (*Moscow, Russ. Fed.*) *56*, 1181–1189.
35. Vinogradov, A. D. (2008) $NADH/NAD^+$ interaction with NADH: ubiquinone oxidoreductase (complex I). *Biochim. Biophys. Acta 1777*, 729–734.
36. Euro, L., Belevich, G., Bloch, D. A., Verkhovsky, M. I., Wikström, M., and Verkhovskaya, M. (2009) The role of the invariant glutamate 95 in the catalytic site of complex I from *Escherichia coli*. *Biochim. Biophys. Acta 1787*, 68–73.
37. Kushnareva, Y., Murphy, A. N., and Andreyev, A. (2002) Complex I-mediated reactive oxygen species generation: Modulation by cytochrome *c* and $NAD(P)^+$ oxidation-reduction state. *Biochem. J. 368*, 545–553.
38. Kudin, A. P., Bimpong-Buta, N. Y.-B., Vielhaber, S., Elger, C. E., and Kunz, W. S. (2004) Characterization of superoxide-producing sites in isolated brain mitochondria. *J. Biol. Chem. 279*, 4127–4135.
39. Mattevi, A. (2006) To be or not to be an oxidase: Challenging the oxygen reactivity of flavoenzymes. *Trends Biochem. Sci. 31*, 276–283.
40. Bücher, T., and Sies, H. (1976) Mitochondrial and cytosolic redox states in perfused rat liver: Methods and problems in metabolic compartmentation. In Use of isolated liver cells and kidney tubules in metabolic studies (Tager, J. M., Söling, H. D., and Williamson, J. R., Eds.) pp 41−64, North-Holland Publishing Co., Amsterdam.
41. Tischler, M. E., Friedrichs, D., Coll, K., and Williamson, J. R. (1977) Pyridine nucleotide distributions and enzyme mass action ratios in hepatocytes from fed and starved rats. *Arch. Biochem. Biophys. 184*, 222–236.
42. Williamson, J. R., and Corkey, B. E. (1979) Assay of citric acid cycle intermediates and related compounds. *Methods Enzymol.,* 200–222.
43. Sies, H. (1982) Nicotinamide nucleotide compartmentation. In Metabolic compartmentation (Sies, H., Ed.) pp 205−231, Academic Press, London.